Journal of Materials Chemistry B

Accepted Manuscript

ROYAL SOCIETY OF CHEMISTRY

www.rsc.org/materialsB

Journal of Materials Chemistry B

ARTICLE

Smart polymeric particles encapsulated gadolinium oxide and europium: Theranostic probe for magnetic resonance/optical imaging and antitumor drug delivery†

Received 00th January 20xx,
Accepted 00th January 20xx

DOI: 10.1039/x0xx00000x
www.rsc.org/

Ruiqing Liu[a, 1], Shuang Liang[b, 1], Cun Jiang[a], Li Zhang[a], Tianmeng Yuan[a], Penghui Li[c,d], Zushun Xu[a], Haibo Xu[b], and Paul K. Chu[c]

Smart polymeric particles possessing the advantages of paramagnetism, luminescence, and controlled drug delivery in a single entity are reported. Gadolinium oxide and europium-encapsulated temperature/pH-responsive polymeric particles (PLTPPs) synthesized by emulsifier-free emulsion polymerization show good biocompatibility with C6 cells and anticancer drug (doxorubicin, DOX) loading capability. *In vitro* drug release assessment discloses release abatement under acidic conditions or at high temperature, and the DOX-loaded PLTPPs have obvious antitumor properties for C6 and H22 cells. Cellular uptake tests confirm that the materials can be taken up by C6 cells to facilitate optical imaging. The T_1-weighted relaxivity value at 3 *T* is 6.13 mM^{-1} s^{-1} which is 39% higher than that of the clinical Magnevist®. *In vivo* MR and optical imaging reveal that the PLTPPs are effectively dual probes. The results indicate that the PLTPPs have great potential in tumor diagnosis and treatment.

1. Introduction

Magnetic resonance (MR) imaging is one of the most popular and effective imaging technique to diagnose tumors due to its high resolution of soft tissue contrast properties but suffers from low sensitivity. [1, 2] In contrast, optical imaging has excellent sensitivity but has low resolution. [2, 3] Therefore, the combination of MR and optical imaging can work synergistically to impart more accurate information about tumor tissues and such dual probes encompassing MR and optical imaging are very attractive. [4-7] Nevertheless, a diagnosis probe (imaging) is insufficient in theranostics and hence, an advanced probe combining MR/optical imaging with drug delivery in a single entity is of technological and clinical significance. [8, 9]

Gadolinium oxide nanoparticles (GONPs) have lower toxicity and higher relaxivity than clinical gadolinium chelates [10-13] and are considered next-generation positive (T_1) MR imaging contrast agents. [14, 15] Compared to quantum dots and organic dyes, europium (Eu)-based optical probes have superior features such as long luminescence lifetime, photostability, narrow emission band width, and large stocks shift. [16-18] Although dual probes based on GONPs and europium for MR/optical imaging have been described, [19, 20] theranostic probes containing GONPs and Eu with dual MR/optical imaging with antitumor drug delivery capability have rarely been reported. Fabrication of dual probes generally involves incorporating Eu(III) into the GONPs host but dual probes synthesized by doping often lack the proper functional group so that they cannot be used as drug carriers. Hence, further introduction of a drug delivery moiety such as poriferous silica and functional polymer is required [21, 22] but simple synthesis of

[a] *Hubei Collaborative Innovation Center for Advanced Organic Chemical Materials, Ministry of Education Key Laboratory for the Green Preparation and Application of Functional Materials, Hubei University, Wuhan 430062, Hubei, China. E-mail: zushunxu@hubu.edu.cn*
[b] *Department of Radiology, Union Hospital, Tongji Medical College, Huazhong University of Science and Technology, Wuhan 430030, Hubei, China. E-mail: xuhaibo1120@hotmail.com*
[c] *Department of Physics and Materials Science, City University of Hong Kong, Tat Chee Avenue, Kowloon, Hong Kong, China. E-mail: paul.chu@cityu.edu.hk*
[d] *Institute of Biomedicine and Biotechnology, Shenzhen Institutes of Advanced Technology, Chinese Academy of Sciences, Shenzhen 518055, China.*
† Electronic supplementary information (ESI) available. See DOI: 10.1039/x0xx00000x
[1] These two authors contributed equally to this work.

GONPs and Eu-based theranostic probes is quite challenging. Therefore, a facile way to synthesize a diagnostic and therapeutic agent based on GONPs and Eu is important.

Tumors generally typically have a more acidic pH or higher temperature than normal tissues [23, 24] and so "smart" drug delivery systems (DDS) that respond to temperature or pH can be used to control the drug release rate. [25] Hence, smart polymer particles responding to the stimuli are promising delivery vehicles for controlled encapsulation and release. [26, 27] In the family of stimuli-responsive polymers, poly(N-isopropylacrylamide) (PNIPAM) (temperature-responsive) and poly(methacrylic acid) (PMAA) (pH-responsive) have attracted much interest on account of their good biocompatibility [28-30] and can be incorporated with GONPs and Eu to fabricate therapeutic probes. Herein, paramagnetic, luminescent, and temperature/pH-responsive polymeric particles (PLTPPs) with simultaneous MR/optical imaging and antitumor drug delivery capability are described (Scheme 1). By means of emulsifier-free emulsion polymerization, GONPs and Eu(III) are introduced to the temperature/pH-responsive polymeric particles. The PLTPPs exhibit good red luminesce, strong MR enhancement, and temperature/pH-responsive dually controlled drug release capacity constituting a multifunctional platform for cancer diagnosis and treatment.

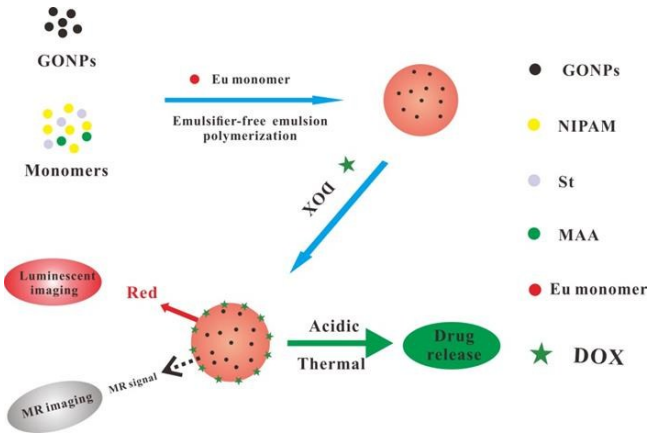

Scheme 1. Illustration of the synthetic process and formation of DOX-loaded PLTPPs.

2. Materials and methods

2.1 Materials

Methacrylic acid (MAA, 99 wt%), N-isopropylacrylamide (NIPAM, 99 wt%), and GONPs (99.99 wt%) were obtained from Aladdin. Styrene (St), potassium peroxydisulfate (KPS) was purchased from Sinopharm Chemical Reagent Co. Ltd., China, and doxorubicin hydrochloride (DOX·HCl) was bought from J&K Scientific. NIPAM and KPS were purified by recrystallization in a toluene/hexane mixture (v/v=1:1) and ultrapure water, respectively. St and MAA were purified by distillation under reduced pressure and stored at 4 °C. All the other reagents were analytical reagent (AR) and used as received.

2.2 Synthesis of PLTPPs

The Eu(III)-monomer was synthesized according to a previously reported method without modification. [31] The smart PLTPPs were synthesized by a facile and environmentally friendly emulsifier-free emulsion polymerization method (Scheme 1). The GONPs (0.806 g) were dispersed in 100 mL of ultrapure water under vigorous agitation and sonication (500 W) for 12 h to form the GONPs dispersion and 7 mL of the GONPs dispersion, MAA (0.2015 g), St (0.5078 g), NIPAM (1.0012 g), and KPS (0.1500 g) were dispersed in 90 mL of ultrapure water, sonicated for 5 minutes (100 W) cooled in an ice bath, and transferred to a 250 mL four-necked round-bottomed flask with a Teflon mechanical stirrer and condenser under flowing nitrogen. It was agitated vigorously at room temperature for half an hour under nitrogen and the mixture was then heated to 78 °C in a water bath. After 45 min, the Eu(III)-monomer (0.08 g) dissolved in 12 mL of ultrapure water was added dropwise. Polymerization (Scheme 2) proceeded for 3 h at 78 °C at a stirring speed of 330 rpm.

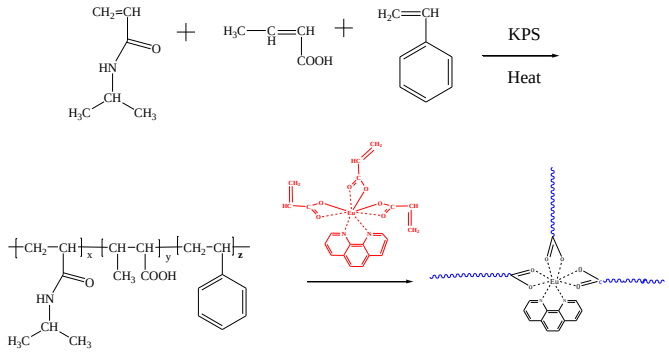

Scheme 2. Illustration of the formation copolymers.

The pure polymeric particles (TPPs) without the GONPs and Eu(III)-monomer were prepared by the same method. All the samples were purified by dialysis (molecular weight cut-off: 14000 Da) against ultrapure water for 7 days and the distilled water was changed with fresh one every 8 hours. To obtain the solid samples and remove the unloaded GONPs, a saturated calcium chloride/methanol solution was added to the purified latex followed by centrifugation at 8000 r min^{-1}. The precipitate was rinsed with distilled water several times and then dried under vacuum at 50 ^{o}C for 48 h.

2.3 Preparation of DOX-loaded PLTPPs

In order to prepare the theranostic probe, the anticancer drug DOX was loaded to the PLTPPs by direct mixing. In brief, 5 mL of the purified PLTPPs latex (50 mg PLTPPs) were diluted with 10 mL of ultrapure water and then 25 mL of the DOX·HCl solution (DOX·HCl 10 mg) were added dropwise, the pH value was sustained near 7.0. The reaction continued overnight in darkness at room temperature at a stirring speed of 200 rpm. The unloaded free drug was removed by dialysis using a dialysis bag (molecular weight cut-off: 14000 Da) against 1000 mL ultrapure water (stirring rate 300 rpm). When the water coming out of the dialysis bag became clear, the DOX-loaded PLTPPs were used to measure the drug loading efficiency (DLE) and the drug loading content (DLC) was determined by UV-vis spectrophotometer. The concentration of DOX·HCl in distilled water was obtained from the calibration curve: c (μg/mL) = (I-0.08706)/0.01630 (R^2 = 0.9998) [32], where I is the UV absorption intensity at 485 nm obtained by subtracting the UV absorbance of the TPPs solution from that of the DOX-loaded PLTPPs. The DLE and DLC were calculated according to the following equations:

DLC (%) = weight of drug encapsulated in PLTPPs/weight of polymer×100%

DLE (%) = weight of drug encapsulated in PLTPPs/weight of drug in feed×100%

2.4 *In vitro* drug release measurements

To investigate the temperature and pH-controlled drug release properties of the PLTPPs, the purified DOX-loaded PLTPPs were put in six new dialysis tubes (molecular weight cut-off: 8 000-10 000 Da, 3 mL/tube) and then a 200 mL beaker containing 150 mL of tris-buffer (0.01 M; pH 5.0 or pH 7.4) for dialysis under stirring at 250 rpm. The six tubes were divided into three groups at 25, 37, and 43 °C, respectively. At the predesigned time intervals, 3.0 mL of the buffer was removed to conduct fluorescence spectroscopy (excitation at 461 nm and emission at 592 nm) to obtain the cumulative drug release curves. The volume of the buffer outside the dialysis tube in the beaker was ensured to be around 150 mL during the measurement. All the above tests were repeated for three times.

2.5 Cytotoxicity test

The cytocompatibility of the PLTPPs and anticancer properties of the DOX-loaded PLTPPs against C6 and H22 cancer cells were evaluated by the standard MTT assay. Both C6 and H22 cancer cells were cloned from the cell line stored by China Center for Type Culture Collection in Wuhan. After incubation of approximately 1 × 10^4 cells in each well of the 96-well plates, various concentrations of the PLTPPs and DOX-loaded PLTPPs were added. The untreated cells served as the control. After incubation for 48 h, 20 μL of MTT (5 mg mL^{-1}) were added to each well and incubated for another 4 h. The supernatant was removed and 150 μL of dimethylsulfoxide were added to each well. The optical density (OD) at 490 nm was measured on a microplate reader and the relative cell viability (%) was calculated by comparing the OD of the experimental group with that of the control group. In order to evaluate the anticancer properties of the DOX-loaded PLTPPs, the relative cell viability of free DOX was also assessed.

2.6 *In vitro* cellular uptake and luminescent imaging

The C6 cells (1×10^5 cells, 1 mL) were seeded on quartz-bottom dish for 24 h at 37 °C. The cells were incubated in a culture medium containing PLTPPs (2 mg mL^{-1}). After incubation for 48 h, the cells were washed with a phosphate buffer solution (PBS) to remove excess PLTPPs and then the nuclei were stained with 40-6-Diamidino-2-phenylindole (DAPI). The cells were imaged in a bright field under excitation of 450-590 nm using an inverted fluorescence microscope (Nikon Eclipse TI-SR).

2.7 *In vitro* T_1-weighted MR imaging

To determine the T_1-weighted relaxivity (r_1), suspensions of the PLTPPs with different gadolinium concentrations (0.10, 0.15, 0.20, 0.25, and 0.30 mM) were determined at room temperature using the Siemens Magnetom Trio 3.0 *T* MR scanner. The samples were transferred to a series of 500 µL tubes and put on a 96-well plate under the MR scanner to obtain different T_1. A linear fit was applied to $1/T_1$ versus Gd(III) concentrations to estimate the relaxivity. The spin-echo pulse sequence was used during the T_1 measurements with the following parameters: Field of view (FOV) = 10×10 cm; Echo time (TE) = 9 ms; Slice thickness = 3 mm. The repetition time (TR) was 300, 400, 500, 600, 800, 1000, 1500, and 2000 ms.

2.8 *In vivo* MR and luminescent imaging

To further measure the potential MR imaging in living organisms, *in vivo* MRI studies were performed on Sprague Dawley (SD) rats weighing approximately 250 g and female Balb/c mice ageing 5 to 6 weeks. Balb/c mice were injected with 100 µL H22 cancer cells. When the tumors reached an approximate size of 150 mm, the mice were used for MR imaging. After the animals were anaesthetized by 10% trichloroacetaldehyde hydrate (35 mg kg^{-1}), they were injected with PLTPPs (dosage 0.04 mmol (Gd) kg^{-1}) through the tail vein and scanned at 3.0 *T* on a clinical MR scanner. The T_1-weighted images were taken at various time points with TR = 106 ms, TE = 4.71 ms, thickness = 3 mm, and averages = 6. The signal intensity (SI) of the organs was obtained from the region of interest (ROI) in the T_1-weighted MR images at the scheduled time points. The relative SI of the organs was calculated using the following formula: SI_{post}/SI_{pre}, where SI_{pre} and SI_{post} represent the signal intensities of the organs before and after injection of the contrast agent, respectively, collected at time points after injection. All the animals were managed and treated according to the rules and regulations of the Institutional Animal Care and Use Committee at Hubei University.

The SD rats were sacrificed 9 hours after post-injection with PLTPPs. The samples taken from the liver, spleen, kidney, and brain were fixed in 4% paraformaldehyde for 24 h and transferred to 30% sucrose in the PBS buffer. The slides of these organs were prepared for confocal laser scanning microscopy (CLSM). The CLSM images were obtained on the Spectra Physics MaiTai HP tunable 2-photon (690-1040 nm) laser confocal microscopy (Carl Zeiss LSM510) using 2-photon laser excitation at 690 nm.

2.10 Characterization

The chemical structure of the PLTPPs was determined by Fourier transform infrared spectroscopy (FTIR, Nicolet IS50 Thermofisher USA) after the dried samples were pressed with KBr and the gadolinium concentration was determined by inductively-coupled plasma optical emission spectrometry (ICP-OES, Optimal 8000 PE, USA). ^{1}H NMR was conducted on the Unity Invoa 600 MHz spectrometer (Varian, USA) with DMSO-d6 as the solvent. The number-average molecular weight (Mn), weight-average molecular weight (Mw) and polydispersity index were measured by gel permeation chromatography (GPC) utilizing the 1515 pump. The morphology and particle size were determined by transmission electron microscopy (TEM, Tecnai G20, FEI Corp. USA) at 200 kV. The samples in water were previously deposited and left for drying on grids. The hydrodynamic diameter was measured on the Zatasizer (ZS90, Malvern UK). The crystal structure of the GONPs and PLTPPs powders was determined by X-ray diffraction (XRD, D8A25, Bruker, Germany) using CuK_a radiation at a scanning rate of 5 °/min. The thermogravimetric analysis was performed on the Perkin-Elmer Diamond TG from 30 °C to 600 °C at a heating rate of 20 °C per minute. The excitation and emission spectra were acquired on the LS-55 spectrometer (PE, USA) and the UV absorption was monitored on a UV-vis spectrophotometer (UV 1800 PC, Mapada, China).

3. Results and Discussion

3.1 Synthesis and characterization of PLTPPs

The smart PLTPPs were synthesized by emulsifier-free emulsion polymerization as illustrated in Scheme 1. The FTIR spectra of TPPs and PLTPPs are shown in Fig. 1. The absorbance band near 3416 cm^{-1} is assigned to the hydroxyl group (-OH) stretching vibrations from water and those at 2973 cm^{-1}, 2883 cm^{-1} are asymmetrical and symmetrical stretching of $-CH_3$ and $-CH_2$, respectively. [33] The characteristic peaks of N-H bending from PNIPAM at 1548 cm^{-1} shift to a smaller wavenumber at 1541 cm^{-1} as a result of copolymerization of NIPAM with St and MAA. The peak at 1711 cm^{-1} arises from C=O stretching of carboxyl groups in PMA and those at 1386 cm^{-1} and 1367 cm^{-1} are associated with isopropyl groups in PNIPAM. [21] The peaks at 3033 cm^{-1} and 708 cm^{-1} are related to stretching and flexural vibration (δ_{C-H}) of the benzene ring in PSt [34] and the absorbance band at 415 cm^{-1} is the characteristic peak of Eu-O stretching (Fig. 1b). The synthesis of the TPPs can be further confirmed by ^1H NMR spectrum [35, 36] (Fig. S1). Furthermore, the number-average molecular weight of TPPs and PLTPPs are 2812 and 4385 Da, respectively (Fig. S2).

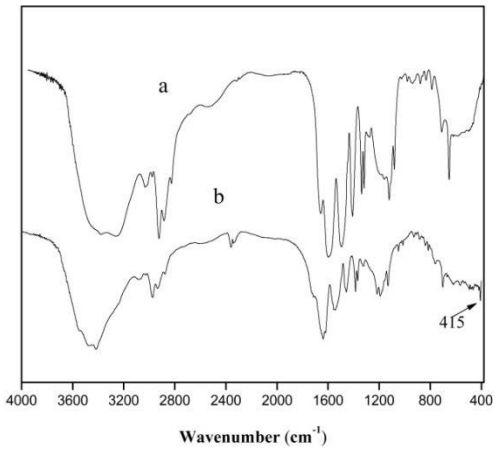

Fig. 1. FT-IR spectra of (a) TPPs, (b) PLTPPs.

The morphology and particle size are determined by transmission electron microscopy (TEM) and dynamic light scattering (DLS). The TEM image in Fig. 2a shows GONPs with a diameter smaller than 20 (±2) nm. The TEM images of TPPs (without GONPs) and PLTPPs are depicted in Figs. 2b and 2c, respectively. Both TPPs and PLTPPs exhibit a spherical shape with a narrow size distribution. As shown in Fig. 2c, the GONPs are encapsulated on the polymer sphere (black dots in the particles) and the average diameter of the PLTPPs (250±5 nm) is larger than that of the TPPs (200±8 nm) due to encapsulation. The average hydrodynamic diameter (D_h) of the PLTPPs is about 462.4 nm. The diameter in an aqueous system (DLS result) is larger than that under dry conditions (TEM result) because of the hydrophilic properties and swelling of the polymeric particles in water. Moreover, the synechia between the particles might be another reason of the difference between the particle size of the PLTPPs measure by TEM and DLS. Encapsulation of GONPs is corroborated by X-ray diffraction (XRD) spectra (Fig. 2d). The peaks are observed at 2θ of about 22°, 26°, 28°, 31° and 32° similar to PLTPPs, indicating that the GONPs are introduced to the PTTPPs as indicated by TEM.

The thermal properties of the PLTPPs are evaluated by thermogravimetric analysis (TGA). As shown in Fig. 2e, the weight loss stage near 100 °C corresponds to the loss of bound water from the polymeric particles and the sharp weight loss from 369 to 433 °C is related to decomposition of the polymer backbone. The last stage in the TGA curves at 433 °C corresponds to the residual weight of gadolinium and europium existing as oxide. There is no residual weight percentage for TPPs at 600 °C and the residual weight percentage of PLTPPs is about 4.3 %. The gadolinium oxide content in the residual is 63 % as determined by ICP-OES.

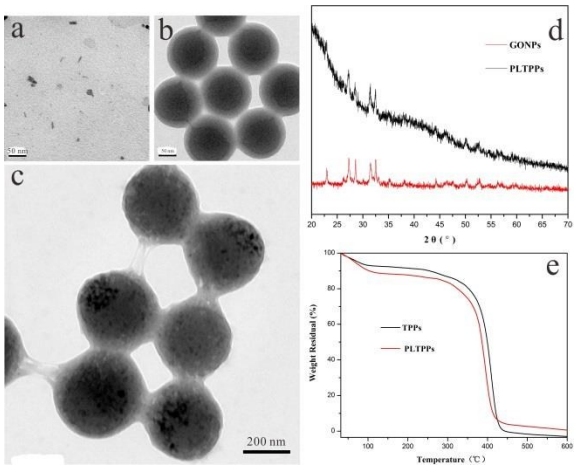

Fig. 2. TEM images: (a) GONPs, (b) TPPs, (c) PLTPPs; (d) XRD spectra. CuK_a radiation at a scanning rate of 5 °/min ; (e) TGA curves. The temperature is from 30 °C to 600 °C at a heating rate of 20 °C per minute.

Furthermore, good stability is indispensable for the biomedical applications of PLTPPs. The stability of PLTPPs is evaluated by DLS. The PTLPPs emulsion is dialyzed against tris-buffer (37 °C) at pH of 5.0 and 7.4 for 7 days and the D_h of the PLTPPs is measured. The D_h of the PLTPPs has no big changes during dialysis (Fig. S3). In addition, the zeta potentials of PLTPPs before (-29.3 mV) and after (-28.6 mV) dialysis have little change, suggesting that the PPPs are stable in this pH range.

3.2 Stimuli-responsive properties

The stimuli-responsive properties have great influence on biomedical applications especially controlled drug delivery. The temperature responsive is evaluated by DLS between 25 and 43 °C. As shown in Fig. 3a, as the temperature is increased, the particle diameter shrinks from 461.5 to 390 nm due to the change in the wettability of the polymers in the aqueous system. It can be attributed to reduction in hydrogen bonds collapsing the polymeric particles and the system transforming into globules. [29, 34] The volume phase transition temperature of PNIPAM is 33 °C as shown in Fig. 3a.

The pH dependence of the PLTPP is investigated. When the pH is increased from 2.3 to 9.1, D_h of the PLTPPs increases to about 100 nm because of the variation in hydrogen bonds and ionization of carboxyl groups (Fig. 3b). D_h exhibits a constant change in the pH range between 4.4 and 7.4 because the pH range is near the reported p*Ka* value of PMAA (~6) , [37] at which the carboxyl groups are ionized and hydrogen bonds decrease. The polymer particles become more hydrophilic and swell. [38] In contrast, when the pH is beyond this range, D_h does not change due to the balance between destruction and formation of hydrogen bonds. Those results indicate that the PLTPPs have good stimuli-responsive properties.

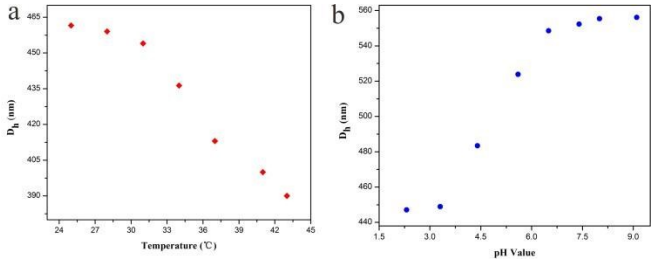

Fig. 3. Hydrodynamic diameters of PLTPPs as a function of (a) temperature and (b) pH.

3.3 Photoluminescence properties

The luminescent properties of the PLTPPs are evaluated by means of the excitation and emission spectra. The emission spectrum was obtained under excitation of 396 nm. As shown in Figs. 4a and 4b, the characteristic transition lines from the $^5D_0$ level of Eu(III) to ^7F_J (J = 2, 4) are observed. The peak at 613 nm corresponds to the $^5D_0$-$^7F_2$ transition and that at 696 nm can be ascribed to the $^5D_0$-$^7F_4$ transition. [21, 39, 40] The excitation spectrum (Fig. 4a) consists of two relatively broad peaks with a maximum at 396 nm and shoulder at 466 nm. [41] To further study the luminescent properties of the PLTPPs, cellular uptake experiments are conducted using fluorescence microscopy. The fluorescenct image clearly shows the uptake and fluorescence of the PLTPPs (red luminesce) (Fig. 4d) by the C6 cancer cells with the nucleus stained with DAPI (Fig. 4c). The luminescent properties and cellular uptake ability suggests that the PLTPPs are good luminescent-labeled probes.

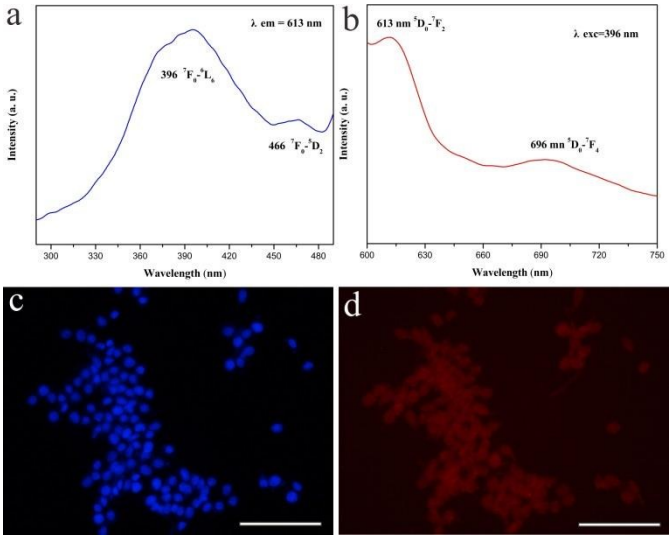

Fig. 4. (a) Photoluminescence excitation spectrum of PLTPPs (λem = 613 nm) and (b) Emission spectrum of PLTPPs (λexc = 396 nm). Inverted fluorescence microscopic images of C6 cells incubated with PLTPPs for 48 h (the nuclei stained with DAPI): (c) bright-field, (d) excitation of 450-590 nm. Bars represent 50 μm

3.4 DOX-loading and *in vitro* release profiles of PLTPPs

DOX loading and *in vitro* release experiments are performed to evaluate the potential application of the polymer vesicles to drug delivery. The DLC and DLE are determined by subtracting

the UV absorbance of the PLTPPs from DOX-loaded PLTPPs at 485 nm. The electrostatic interactions between the -COO^- groups of PMAA and -NH_3^+ of DOX·HCl drive the loading process. The drug loading content is about 9.5 wt%, DLE is about 46.7 wt%, and DOX concentration is about 159 μg mL^{-1}.

To evaluate the effecst of the solution pH and temperature on the release profile of the PLTPPs, the DOX-loaded particles are placed under different acidic conditions and at different temperature. Since tumors generally exhibit a more acidic pH or higher temperature [23], six sets of pH and temperature conditions are selected in this study: (1) pH = 7.4 and T = 25 °C, (2) pH = 7.4 and T = 37 °C, (3) pH = 5.0 and T = 25 °C, (4) pH = 5.0 and T = 37 °C, (5) pH = 5.0 and T = 43 °C, (6) pH = 7.4 and T = 43 °C. Fig. 5 displays the *in vitro* release profiles of the DOX-loaded PLTPPs. After dialysis for 55 h, 89.6% (± 0.5%)of the drugs are released from the PLTPPs at a pH of 5.0 at 37 °C and it is 2.8 times higher than that at a pH of 7.4 (32.1± 0.1%). This can be attributed to protonation of the -COO^- groups in the PMAA chains at a pH of 5.0 thereby accelerating DOX ($pKa_{DOX·HCl}$=8.25) [42] release from the polymeric particle corona. When a pH of 5.0, the DOX release rate at 43 °C is 15.6 % larger than that at 25 °C which is lower than the LSCT of PLTPPs (~33 °C). When the temperature is increased above the LSCT, the polymer chains become hydrophobic and the polymeric particles shrink. It means that the "door" is open to a maximum extent and drugs can be released. [24] In contrast, when the pH drops from 7.4 to 5.0 and temperature is increased from 25 to 43 °C simultaneously, the DOX release percentage is improved to 78.5 % and reaches 95.3 % (±1.0%), which is much larger than that reported from other single-stimuli controlled drug release polymer systems. [32, 43, 44]

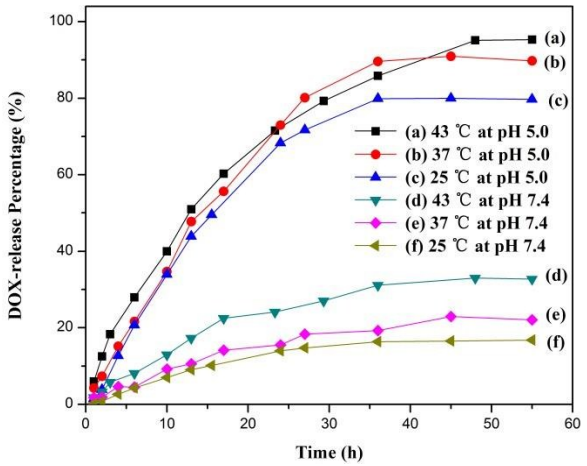

Fig. 5. Cumulative drug release profiles of DOX-loaded PLTPPs in tris-buffer (0.01M) at the condition of (a) 43 ℃ at pH 5.0, (b) 37 ℃ at pH 5.0, (c) 25 ℃ at pH 5.0, (d) 43 ℃ at pH 7.4, (e) 37 ℃ at pH 7.4, and (f) 25 ℃ at pH 7.4. All the standard deviation (SD) are not more than 1.0 %.

3.5 Cytotoxicity Tests

The cytocompatibility of the PLTPPs is an important factor concerning *in vivo* applications and is determined by MTT against C6 cancer cells. The PLTPPs with different concentrations are incubated with C6 cells for 48 hours and the relative cell viability is calculated by measuring the optical density. In the concentration range, all the relative cell viability is above 85% (Fig. 6), suggesting good cytocompatibility boding well for applications *in vivo*.

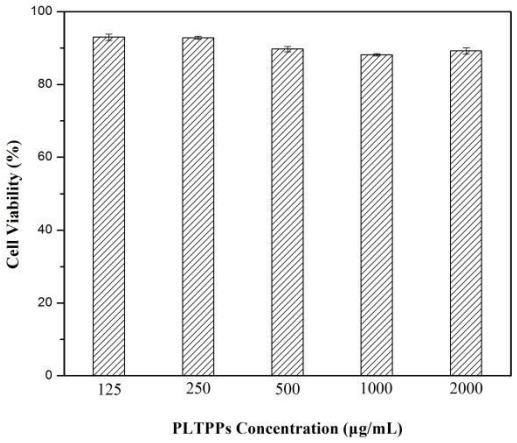

Fig. 6. Cell viability against C6 cells assessed by MTT assay.

In order to show whether the DOX-loaded PLTPPs can be used as anticancer drugs, the *in vitro* anticancer properties are studied on C6 cells *via* the cell viability assay with free DOX as the control. As shown in Fig. 7, the cell viability decreases

significantly when the cells are treated with DOX-loaded PLTPPs. The necessary concentration for effective therapy (cell viability of cells is less than 40 %) is 5 μg mL^{-1}. The DOX concentration in the PLTPPs is 159 μg mL^{-1} and the drug release rate is about 89.6 %. The final concentration of DOX released from the PLTPPs is as high as 140 μg mL^{-1}, which is much higher than the essential concentration. The cytocompatibility and anticancer ability of PLTPPs against H22 cells are also investigated, similar results to that against C6 cells are found (Fig. S4 and S5), which indicate that the PLTPPs not only effective for one kind cells. The good cytocompatibility of PLTPPs and effective anticancer ability of the DOX-loaded PLTPPs bode well for cancer therapy.

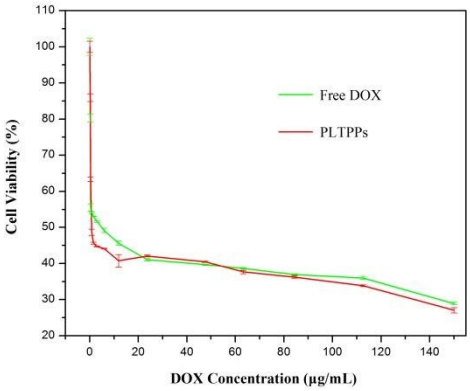

Fig. 7. Antitumor activity of DOX-loaded PLTPPs against C6 cells *via* the cell viability assay with free DOX as the control.

3.6 *In vitro* MR imaging

In order to examine the paramagnetic behavior of the PLTPPs and their application as positive MR contrast agents, MR imaging and relaxation time measurements based on Gd(III) concentrations are performed on a clinical 3.0 *T* MR scanner. As shown in Fig. 8, as the Gd(III) concentration is increased (from right to left), the T_1-weighted maps show a gradual increase in brightness (a higher concentration of Gd(III) produced a brighter signal) and the longitudinal relaxivity (r_1) is 6.13 mM^{-1} s^{-1} which is 39% larger than that of clinical Magnevist® (r_1=4.43 mM^{-1} s^{-1}).

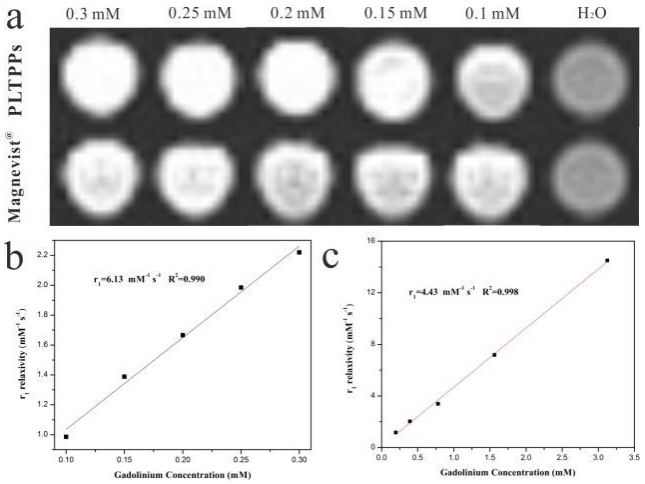

Fig. 8. (a) T_1-weighted *in vitro* MR imaging of PLTPPs and Magnevist®. The relaxivity of (b) PLTPPs and (c) Magnevist®. The longitudinal relaxation time (T_1) is measured on a clinical 3.0 *T* MR scanner at various Gd(III) concentrations.

3.7 *In Vivo* MR/optical Imaging

Owing to the complementary naturey of MR and optical imaging, a dual probe is important to cancer diagnosis. To further investigate MR and optical imaging ability *in vivo*, the PLTPPs are injected into SD rats through the tail vein and they undergo scanning on a 3.0 *T* clinical MR scanner. The T_1-weighted MR images are collected at different time points. As shown in Fig. S6, at 15 min post-injection, a brighter signal is observed from the organs (liver and spleen) and after 2 h, the brightest T_1-weighted MR images are obtained. At 6 hours post-injection, the PLTPPs still show good enhancement, indicating that the circulation time of the PLTPPs *in vivo* is long enough for MRI. However, when the PLTPPs are injected into tumor bearing mice, the relative signal in tumor site is much higher than that in the main organs such as liver (Fig. 9), which indicates the special affinity of PLTPPs to the tumor. This is of great significance for the possible therapy.

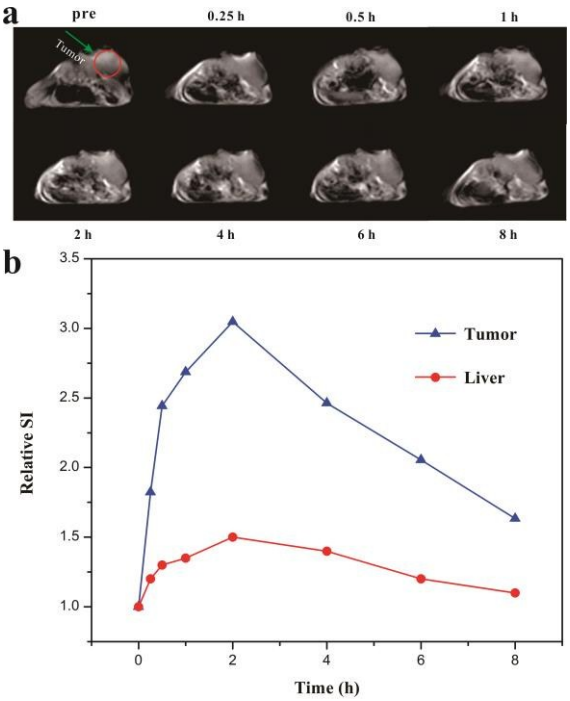

Fig. 9. (a) T_1-weighted mice MR images taken at time points of 0, 0.25, 0.5, 1, 2, 4, 6, and 8 h and (b) relative SI of tumor and liver.

To further assess the optical imaging properties of the PLTPPs, the rats are sacrificed 9 hours after injection and the slides of major organs are prepared for CLSM imaging. The PLTPPs indicate characteristic vivid red luminescence from Eu(III) under 2-photon 690 nm (Fig. 10) confirming that the PLTPPs constitute an effective dual probe for MR/optical imaging.

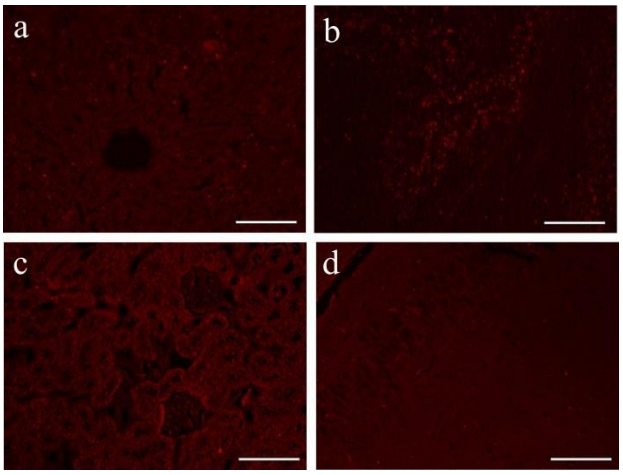

Fig. 10. CLSM images: (a) Liver, (b) Spleen, (c) Kidney, and (d) Brain after injection with PLTPPs. The CLSM images were obtained using 2-photon laser excitation at 690 nm. Bars represent 50 μm

4. Conclusion

Theranostic probe containing GONPs and Eu(III) filled with the thermo/pH-responsive polymer as the temperature/pH-controlled switch is designed and fabricated. Different from the conventional synthetic route, the polymerization reaction to encapsulate GONPs and conjugate Eu-monomer occurs at the same time and a single procedure suffices. The polymeric particles have good biocompatibility and DOX-delivery ability as demonstrated by the slow release under neutral conditions but fast release under acidic conditions or at a high temperature. Moreover, they have excellent photoluminescence properties delivering good performance in *in vitro* and *in vivo* optical imaging. The good magnetic contrast of these particles underscores their good potential as robust MRI probes. All in all, the fabrication procedures are simple and readily upscalable. Boasting efficient optical and MR imaging along with the drug delivery and controlled release capabilities, these smart polymeric particles are useful in new-generation of theranostic probes in clinical applications.

Acknowledgements

This work was financially supported by the National Natural Science Foundation of China (Grant NO. 51573039, 81171386, 81372369, 31500773), City University of Hong Kong Strategic Research Grant (SRG) No. 7004188, and Hong Kong Research Grants Council (RGC) General Research Funds (GRF) No. CityU 112212.

References

1. M. Rudin and R. Weissleder, *Nat. Rev. Drug. Discov.*, 2003, **2**, 123-131.
2. S. M. Janib, A. S. Moses and J. A. MacKay, *Adv. Drug. Deliv. Rev.*, 2010, **62**, 1052-1063.
3. R. Weissleder and M. J. Pittet, *Nature*, 2008, **452**, 580-589.
4. X. Xing, B. Zhang, X. Wang, F. Liu, D. Shi and Y. Cheng, *Biomaterials*, 2015, **48**, 16-25.
5. H. Chen, G. D. Wang, W. Tang, T. Todd, Z. Zhen, C. Tsang, K. Hekmatyar, T. Cowger, R. B. Hubbard, W. Zhang, J. Stickney, B. Shen and J. Xie, *Adv. Mater.*, 2014, **26**, 6761-6766.
6. V. Caratto, F. Locardi, G. A. Costa, R. Masini, M. Fasoli, L. Panzeri, M. Martini, E. Bottinelli, E. Gianotti and I. Miletto, *ACS Appl. Mater. Interfaces*, 2014, **6**, 17346-17351.
7. J. Liu, J. Bu, W. Bu, S. Zhang, L. Pan, W. Fan, F. Chen, L. Zhou, W. Peng, K. Zhao, J. Du and J. Shi, *Angew. Chem. Int. Ed. Engl.*, 2014, **53**, 4551-4555.
8. T. Krasia-Christoforou and T. K. Georgiou, *J. Mater. Chem. B*, 2013, **1**, 3002.
9. Y. Liu and N. Zhang, *Biomaterials*, 2012, **33**, 5363-5375.
10. M. Cho, R. Sethi, J. S. Narayanan, S. S. Lee, D. N. Benoit, N. Taheri, P. Decuzzi and V. L. Colvin, *Nanoscale*, 2014, **6**, 13637-13645.
11. X. H. Ma, A. Gong, L. C. Xiang, T. X. Chen, Y. X. Gao, X. J. Liang, Z. Y. Shen and A. G. Wu, *J. Mater. Chem. B*, 2013, **1**, 3419-3428.
12. N. Luo, X. Tian, C. Yang, J. Xiao, W. Hu, D. Chen and L. Li, *Phys. Chem. Chem. Phys.*, 2013, **15**, 12235-12240.
13. J. Y. Park, M. J. Baek, E. S. Choi, S. Woo, J. H. Kim, T. J. Kim, J. C. Jung, K. S. Chae, Y. Chang and G. H. Lee, *ACS Nano*, 2009, **3**, 3663-3669.
14. Y. Shao, X. Tian, W. Hu, Y. Zhang, H. Liu, H. He, Y. Shen, F. Xie and L. Li, *Biomaterials*, 2012, **33**, 6438-6446.
15. J. Fang, P. Chandrasekharan, X. L. Liu, Y. Yang, Y. B. Lv, C. T. Yang and J. Ding, *Biomaterials*, 2014, **35**, 1636-1642.
16. Q. Ju, D. Tu, Y. Liu, R. Li, H. Zhu, J. Chen, Z. Chen, M. Huang and X. Chen, *J. Am. Chem. Soc.*, 2012, **134**, 1323-1330.
17. J. Jung, M. A. Kim, J.-H. Cho, S. J. Lee, I. Yang, J. Cho, S. K. Kim, C. Lee and J. K. Park, *Biomaterials*, 2012, **33**, 5865-5874.
18. L. Pellegatti, J. Zhang, B. Drahos, S. Villette, F. Suzenet, G. Guillaumet, S. Petoud and É. Tóth, *Chem. Commun. (Camb)*, 2008, DOI: 10.1039/b817343e, 6591-6593.
19. S. Majeed and S. A. Shivashankar, *J. Mater. Chem. B*, 2014, **2**, 5585-5595.
20. Z. Hu, M. Ahren, L. Selegard, C. Skoglund, F. Soderlind, M. Engstrom, X. Zhang and K. Uvdal, *Chemistry*, 2013, **19**, 12658-12667.
21. X. Kang, Z. Cheng, D. Yang, P. a. Ma, M. Shang, C. Peng, Y. Dai and J. Lin, *Adv. Funct. Mater.*, 2012, **22**, 1470-1481.
22. M. H. Chan and H. M. Lin, *Biomaterials*, 2015, **46**, 149-158.
23. D. Schmaljohann, *Adv. Drug. Deliv. Rev.*, 2006, **58**, 1655-1670.
24. X. Wu, Z. Wang, D. Zhu, S. Zong, L. Yang, Y. Zhong and Y. Cui, *ACS Appl. Mater. Interfaces*, 2013, **5**, 10895-10903.
25. J. Yu, X. Chu and Y. Hou, *Chem. Commun. (Camb)*, 2014, **50**, 11614-11630.
26. J. Tang, Y. Sheng, H. Hu and Y. Shen, *Prog. Polym. Sci.*, 2013, **38**, 462-502.
27. G. L. Davies, I. Kramberger and J. J. Davis, *Chem. Commun. (Camb)*, 2013, **49**, 9704-9721.
28. H. G. Schild, *Prog. Polym. Sci.*, 1992, **17**, 163-249.
29. A. Chan, R. P. Orme, R. A. Fricker and P. Roach, *Adv. Drug. Deliv. Rev.*, 2013, **65**, 497-514.
30. K. Y. Lee and D. J. Mooney, *Chem. Rev.*, 2001, **101**, 1869-1880.
31. X. X. Hu, P. H. Li, K. W. K. Yeung, P. K. Chu, S. L. Wu and Z. S. Xu, *J. Polym. Sci. A*, 2010, **48**, 5961-5967.
32. Q. Liu, S. Chen, J. Chen and J. Du, *Macromolecules*, 2015, **48**, 739-749.
33. J. Peng, T. Qi, J. Liao, M. Fan, F. Luo, H. Li and Z. Qian, *Nanoscale*, 2012, **4**, 2694-2704.
34. H. Zhu, J. Tao, W. Wang, Y. Zhou, P. Li, Z. Li, K. Yan, S. Wu, K. W. Yeung, Z. Xu, H. Xu and P. K. Chu, *Biomaterials*, 2013, **34**, 2296-2306.

35. E. Díez-Peña, I. Quijada-Garrido, J. M. Barrales-Rienda, I. Schnell and H. W. Spiess, *Macromolecular Chemistry and Physics*, 2004, **205**, 438-447.

36. T. Hoare and R. Pelton, *Langmuir*, 2004, **20**, 2123-2133.

37. E. Kharlampieva and S. A. Sukhishvili, *Macromolecules*, 2003, **36**, 9950-9956.

38. J. Kost and R. Langer, *Adv. Drug. Deliv. Rev.*, 2012, **64**, 327-341.

39. J. Liu, X. Tian, N. Luo, C. Yang, J. Xiao, Y. Shao, X. Chen, G. Yang, D. Chen and L. Li, *Langmuir*, 2014, **30**, 13005-13013.

40. M. C. Heffern, L. M. Matosziuk and T. J. Meade, *Chem. Rev.*, 2014, **114**, 4496-4539.

41. M. Abdesselem, M. Schoeffel, I. Maurin, R. Ramodiharilafy, G. Autret, O. Clement, P. L. Tharaux, J. P. Boilot, T. Gacoin, C. Bouzigues and A. Alexandrou, *ACS Nano*, 2014, **8**, 11126-11137.

42. A. Choucair, P. L. Soo and A. Eisenberg, *Langmuir*, 2005, **21**, 9308-9313.

43. Q. Liu, H. Zhu, J. Qin, H. Dong and J. Du, *Biomacromolecules*, 2014, **15**, 1586-1592.

44. Y. T. Chiang and C. L. Lo, *Biomaterials*, 2014, **35**, 5414-5424.

Paramagnetic, luminescent, and temperature/pH-responsive polymeric particles with MR/optical imaging and antitumor drug delivery capability are prepared by emulsifier-free emulsion polymerization.